Extra-Long C-C Single Bonds via Negative Hyperconjugation in Perfluoropinacolate Complexes

Paul A. Homuth,[a] James McNeely,[a] Linda H. Doerrer[a, *]

[a] Department of Chemistry, Boston University, 590 Commonwealth Avenue, Boston, Massachusetts 02215

*Corresponding author: doerrer@bu.edu

Abstract

A computational study on a series of pinacolate ligands with varying degrees of fluorination (from four to zero CF_3 groups) has been carried out to understand the exceptionally long central C-C bonds in crystal structures with the perfluoropinacolate ligand, {A(pin^F)}. The systems were studied with both DFT (PBE0) and *ab-initio* (MP2 NEVPT2) models to elucidate the features of the electronic structure responsible for the enhanced central bond routinely observed in {A(pin^F)} species. Two main influences are responsible: (i) negative hyperconjugation exists between the alkoxide O atom lone pairs and the central C-C σ^* bond which also have resonance forms that formally break the central C-C bond and (ii) the lack of hydrogen bonding between any C-H bonds and the ligand O atoms. Steric influences do not play a significant role, but a central atom A with a point charge of at least plus two bound to pin^F is required to reproduce the crystallographically determined C-C distances.

*Dedicated to Prof. Arnold L. Rheingold for decades of peerless collaboration, hundreds of single crystal X-ray diffraction data sets, and invaluable discussions about what the data actually mean.

Introduction

Numerous transition metal, rare-earth, and *p*-block metal complexes of the perfluoropinacolate (pin^F) ligand have been prepared by our group[1-9] and others, particularly those of Willis[10] and Klüfers.[11-16] In every case, the central C-C bond is exceptionally long compared to a typical single C-C bond length of 1.54 Å. An overview of known, structurally-characterized compounds in the Cambridge Structural Database[17] is given in Scheme 1. For 115 unique distances in 60 metal-containing structures, the average C-C distance is 1.63(3) Å. For 46 unique distances in 31 non-metal containing structures, the average distance is 1.60(1) Å. Herein we report a computational study that elucidates the electronic structure reasons for this difference.

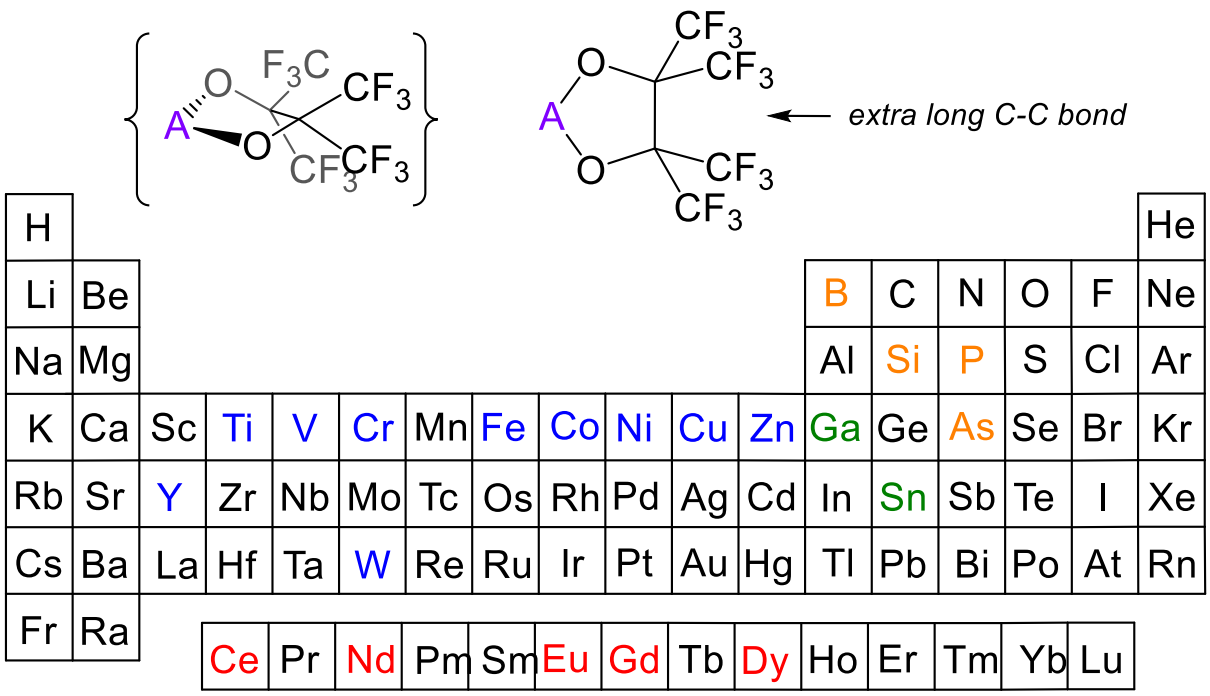

Scheme 1. Summary of compounds containing {A(pin^F)} moieties with indicated coordinating atoms A. Colored elements indicate structurally characterized examples.

Computational Methods

Unless otherwise noted, all electronic structure calculations were performed with ORCA, version 4.1.[18-21] A number of different theoretical models were benchmarked to determine the most economic method for obtaining an accurate geometry for the perfluoropinacolate $(pin^F)^{2-}$ ligand. The models were benchmarked against a structure obtained at the RI-SCS[22-24]-MP2/ma[25]-DEF2-QZVPP[26] level with an automatically generated auxiliary basis set[27]. It was found that RI-MP2/DEF2-TZVP geometries provided good performance with manageable costs. A full description of the benchmarking can be found in Table S1.

The wavefunctions were analyzed with tools provided by NBO 7.0[28], Multiwfn[29], and JANPA[30, 31]. Multiwfn was used to perform topological analysis. Extensive use has been made of second-order perturbative estimates provided by NBO to quantify interactions between orbitals, as well as STERIC analysis and NPA provided by NBO. NBO 7.0 was also used for all Natural Resonance Theory (NRT) analyses.

Potential energy surfaces of $(pin^F)^{2-}$ complexed with point charges were modeled at the FIC-NEVPT2(2,2)[32]/DEF2-TZVP//CASSCF(2,2)/DEF2-TZVP level in order to adequately handle any significant static correlation that might present itself during the scan. The active space consisted of two electrons correlated with the central C_1-C_2 σ and σ* bonds.

Results

A series of pinacolate dianions with a range of fluorinations from fully fluorinated to fully hydrogenated was used in this study and are shown in Scheme 2. Compound **1** is the fully fluorinated dianionic form $(pin^F)^{2-}$ from the crystal structures mentioned above with twelve F atoms in four CF_3 groups. Compound 2 has zero F atoms and is the simple pinacolate dianion, $(pin^H)^{2-}$. In between are the anions with three CF_3 groups (compounds 3A and 3B), two CF_3 groups (4A, 4B, 4C, and 4D). and one CF_3 group (5A and 5B).

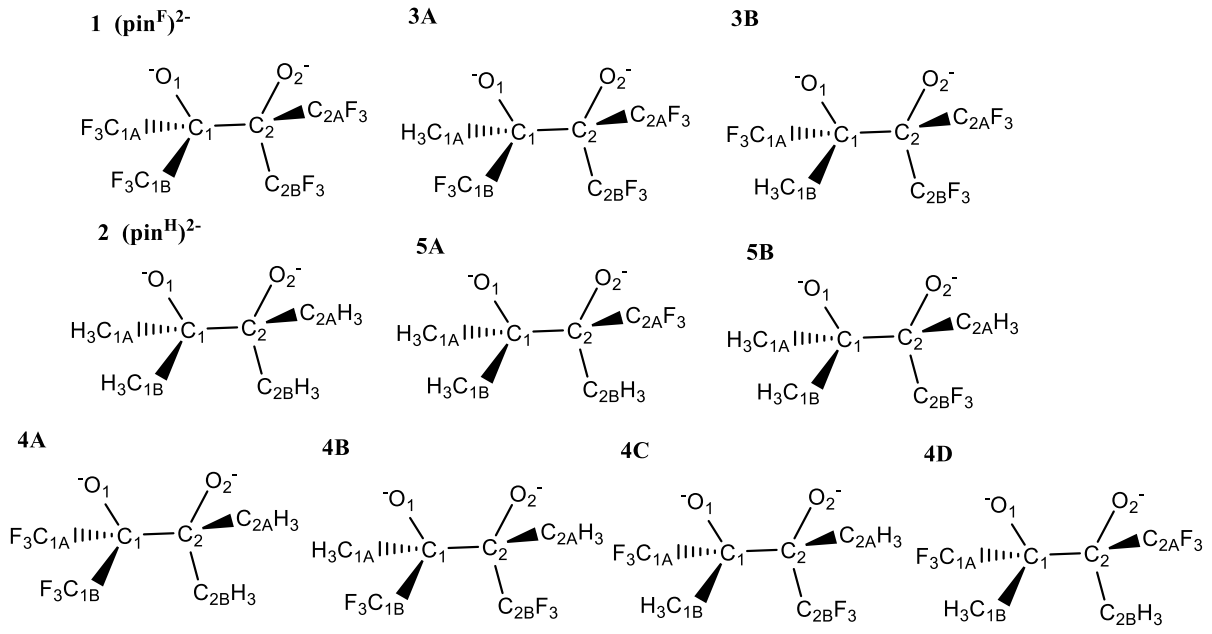

Scheme 2. Labeling scheme used in this work.

In the literature,[17] there are more than 1700 structurally characterized examples of {B(pin^H)} with central C-C bonds averaging 1.55(3) Å. There are only 31 structurally characterized examples of {TM(pin^H)} chelate rings with transition metals having an average C-C distance of 1.53(5) Å, which clearly indicates that the size of the centrally bound atom does not have a strong lengthening effect on the C-C bond. We are not aware of any structurally characterized pinacolate ligands with any intermediate degree of fluorination.

*Comparison of perfluoropinacolate (pin^F)$^{2-}$ (**1**) vs. pinacolate (pin^H)$^{2-}$ (**2**)*

As discussed in the introduction, the length of the C_1-C_2 bond that anchors the (pin^F)$^{2-}$ ligand is unusually long. We calculated this bond in the dianion **1** alone to be 1.761 Å, with a O_1-C_1-C_2-O_2 dihedral angle of 42.9°. For **2**, the C_1-C_2 bond is reduced to 1.627 Å and the O_1-C_1-C_2-O_2 dihedral angle increases to 80.5°. When comparing the structural parameters for **1** with experimental parameters measured for (pin^F)$^{2-}$ in [Co(II)(pin^F)(PPh$_3$)$_2$] (Table S17), the central C-C bond length

in **1** is significantly longer by 11 pm .[33]. It will be shown (*vide infra*) that this lack of agreement is not due to a failure of our theoretical model, but rather a result of the alteration of the electronic structure of $(pin^F)^{2-}$ when ligated to metal centers or point charges.

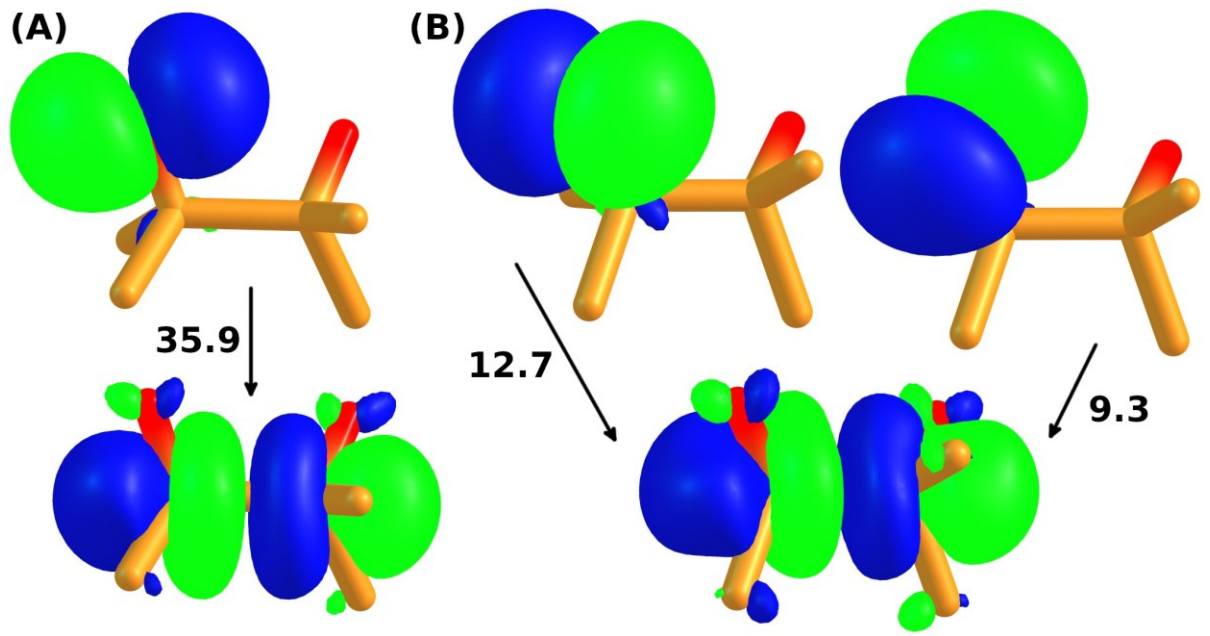

Figure 1. Interaction of oxygen lone pair orbitals with C_1-C_2 bonds for **1** (A) and **2** (B). Delocalization energies given in kcal/mol and include contributions from both donor atoms (O_1+O_2).

The electronic structure of **1** calculated with unrelaxed densities at the RI-MP2/DEF2-TZVP level is largely consistent with the Lewis structure shown in Scheme 1. The oxygen atoms are calculated to have natural charges of -0.88, the fluorine atoms have natural charges that range between -0.33 and -0.39, the central C_1/C_2 atoms possess a natural charge of +0.14, and the ancillary CF_3 carbons, C_{1A}-C_{2B}, were shown to have charges of 0.95-0.96. The C_1-C_2 bond order was found to be 0.72, the $C_{1A\text{-}2B}$-F bond orders ranged between 0.77-0.84, the $C_{1,2}$-O bond order was found to be 1.14, and the $C_{1,2}$-$C_{1A\text{-}2B}$ bond orders ranged between 0.82-0.84.

The enhanced bond order observed for $C_{1,2}$-O and the corresponding reduction in the C_1-C_2 bond order are worth discussing at this point. The benchmarking discussed in the computational methods section revealed that several of the computational models that were explored 'broke' the C_1-C_2 bond. For comparison, it is observed that the C_1-C_2 bond order increases to 0.80 and the $C_{1/2}$-O bond order decreases to 1.04 for compound **2** which is fully hydrogenated. These features are also represented in topological analyses as shown in Table S16.

Clearly the -CF_3 groups present in **1** are expected to pull electron density away from the central C_1-C_2 bond, and thus reduce the observed bond orders relative to **2**. This difference should present in the $\sigma(C_1\text{-}C_2) \rightarrow \sigma^*(\text{C-F/H})$ delocalization energies as determined by NBO second-order perturbative estimates. Indeed, the stabilization induced by these delocalizations increases from 6.5 to 12.7 kcal/mol when moving from **2** to **1** at the PBE0/DEF2-TZVP//RI-MP2/DEF2-TZVP level. (Figure S2)

What is less clear is the reason for the natural charge differences observed for C_1/C_2 in **1** versus **2**. One might expect based on the delocalization described above and the electron-withdrawing power of the -CF_3 groups in **1** that the natural charge of the C_1/C_2 atoms in **2** would be less positive than for **1**. However, the opposite is true. The C_1/C_2 natural charge increases from +0.14 in **1** to +0.28 in **2**. One possible mechanism for this enhanced electron density on the C_1/C_2 atoms in the fluorinated ligand is negative hyperconjugation between the fluorine lone pairs and the C_1-C_2 σ^* bond, as shown on the left of Scheme 3, but analysis of the 2nd order NBO delocalizations eliminates this possibility. Furthermore, other studies of negative hyperconjugation with fluorinated alkanes suggest that this phenomenon is most likely to occur in the opposite direction [$X \rightarrow \sigma^*$(C-F)] from what was proposed above [$F \rightarrow \sigma^*$(C-F)].[34-36]

Interestingly, the negative hyperconjugation between *oxygen* lone pairs and the C_1-C_2 σ* bond,

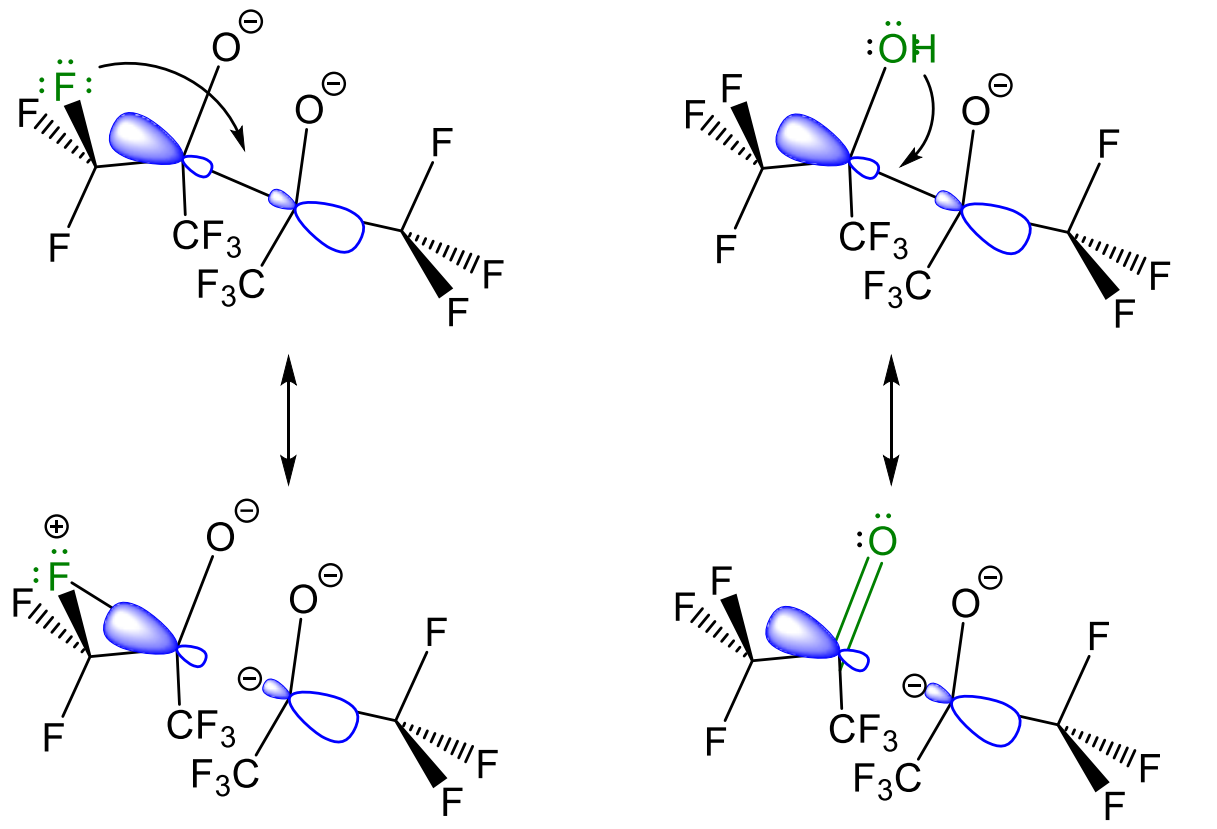

Scheme 3. Negative hyperconjugation between F lone pairs (left) and O lone pairs (right) and the central C-C σ* orbital. .

on the right of Scheme 3, appears to be responsible for the $C_{1,2}$ natural charge discrepancy between **1** and **2**. As seen in Figure 1 above, the stabilization induced by interaction between the

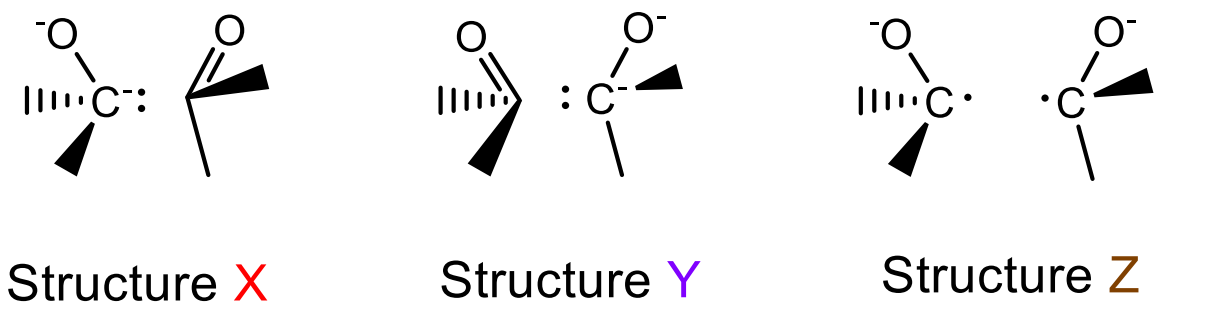

Scheme 4. Three different representative structures used in NRT analysis for different distribution of charge upon central C-C bond cleavage.

oxygen lone pairs and the C_1-C_2 σ* bond increases by ~7 kcal/mol for each donor atom when moving from **2** to **1**. In this Figure, part A on the left depicts donor-acceptor interaction from the O_1 lone pair to the C_1-C_2 σ* orbital, with the cumulative stabilization obtained from O_1+O_2 donation shown next to the arrow for **1**. Part B on the right shows the same features for **2**. This interaction would naturally lead to an increase in the backbone bond length.

14.78, 1.03, 14.80

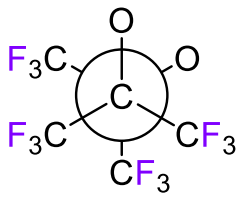

Compound 1

10.26, 10.29

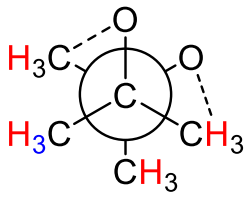

Compound 2

13.97, 7.94

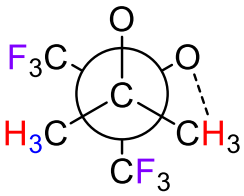

Compound 4A

11.66, 11.66

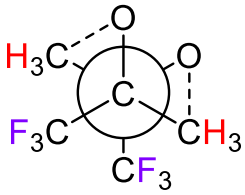

Compound 4B

11.95, 10.26

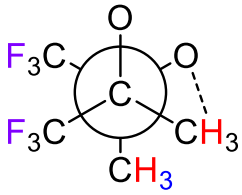

Compound 4C

9.08, 4.20, 9.05

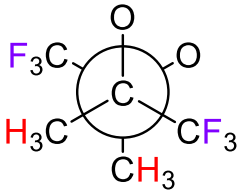

Compound 4D

12.24, 11.93

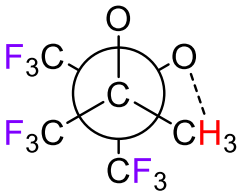

Compound 3A

11.78, 9.55

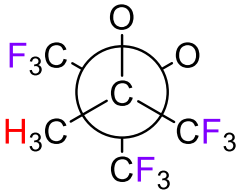

Compound 3B

11.32, 10.34

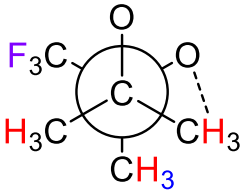

Compound 5A

14.22, 8.19

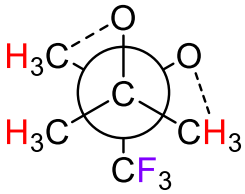

Compound 5B

Figure 2. NRT summary for **1-5B**. Numbers above structures (X,(Z,)Y) refer to weight of resonance structures from Scheme 4 in which charge has been transferred to the C_1 fragment (X), C_2 fragment (Y), or distributed across both fragments after cleaving the C_1-C_2 bond.

The enhancement of the $n_O \rightarrow \sigma^*$ interactions between the O lone pairs and the C_1-C_2 σ^* orbital can also be rationalized as a stabilization of resonance forms for **1** in which the central C_1-C_2 bond has been cleaved, depicted as structures X Y, and Z in Scheme 4, and should be discernable from Natural Resonance Theory (NRT) analysis. The results for **1**-**5B** are shown in Figure 2 which indicates above each compound two or three sums of NRT weights depicted as representative resonance structures X, Y, and Z, that result from distribution of charge after cleavage of the central C-C bond. As can be seen in Figure 2, as CF_3 groups are successively replaced with CH_3 groups, the weight of these resonance forms systematically decreases, and the migration of the charge depends on the presence of -CH_3 groups on the relevant fragment. The weight of these resonance forms also corresponds with the modeled bond length, bond order, and natural charge assignments that were observed (*vide infra*). Fluorination of the terminal groups is expected to help stabilize the charge transfer associated with these resonance forms by helping to delocalize the charge. This can clearly be seen by inspecting the resonance forms in Tables S2-S11.

Methyl Substitution

Given the results from the above section, we have systematically studied the effect of replacing the CF_3 groups in **1** with CH_3 groups on the geometry and electronic structures. We have already discussed how the NRT weights vary with changes in fluorination, but a more thorough discussion is warranted to gain insight into conformational effects on the electronic structure, and to investigate robustly the interplay between the electron-withdrawing power of the terminal CX_3 groups and the geometric/electronic structure of the molecular backbone.

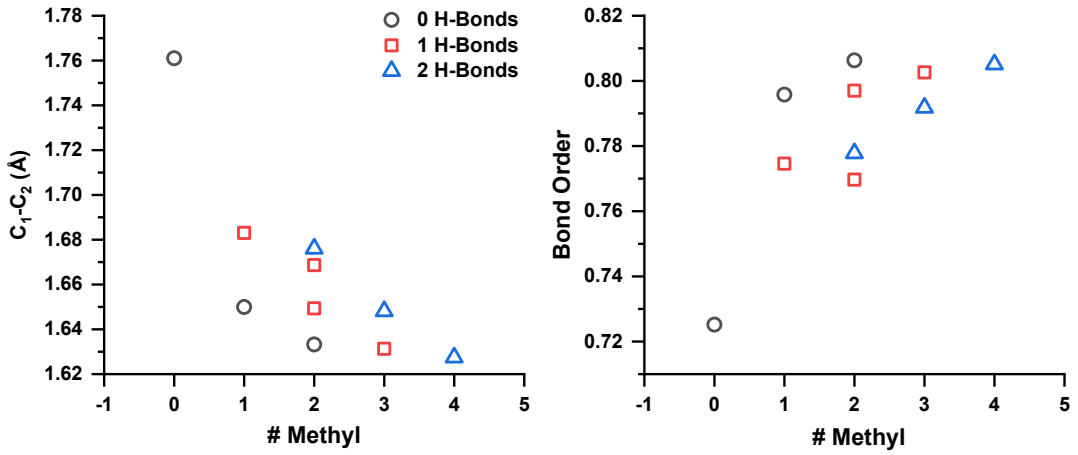

Figure 3. Correlation of C_1-C_2 bond length (a) and bond order (b) versus number of methyl groups. Symbol shape and color [see legend] highlight the trends with respect to the number of CH_3-O hydrogen bonds present in the system.

Analysis of both Figure 2 and Figure 3 highlights another feature that stabilizes the resonance forms that reduce the C_1-C_2 bond order and lengthen the bond. The data suggest that the ability of the CH_3 groups to hydrogen bond with the keto oxygen atoms adds additional stabilization. These interactions are indicated with dotted lines in the Newman projections of Figure 2. This benefit is due to the ability of the hydrogen bond to dissipate further some of the negative charge that has now been localized on one of the fragments in the resonance forms. The color coding in Figure 3 illustrates how the correlation between the C_1-C_2 bond length (left)/bond order (right) and the number of $–CH_3$ groups is slightly improved when grouping the data points into classes that depend on the number of hydrogen bonds in the molecule. An analysis of steric interactions in these systems has been conducted, but the interactions were unremarkable, as can be seen in Tables S28 and S29.

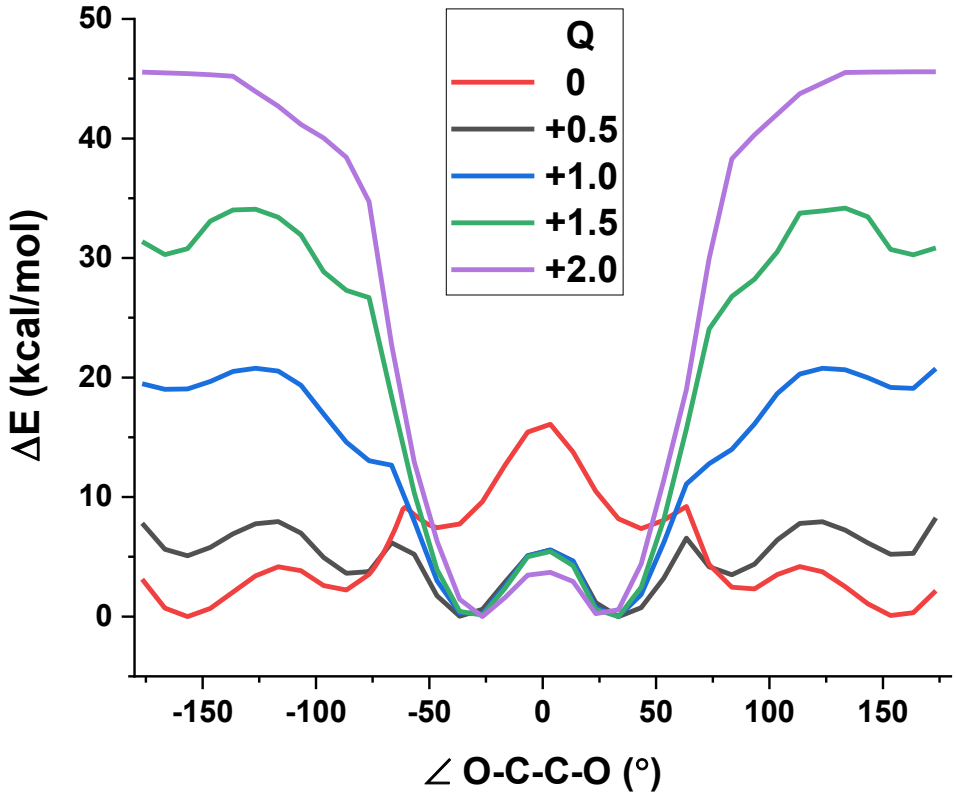

Figure 4. Potential energy surfaces for O-C-C-O dihedral angle with point charges of 0, +0.5,+1.0, +1.5, and +2.0 present. PESs performed at the NEVPT2(2,2)/DEF2-TZVP//CASSCF(2,2)/DEF2-TZVP level.

Introduction of Point Charges

At the start of the results section, we remarked that the bond length calculated for the dianionic form **1** is significantly longer than those that are normally observed in experimental structures of $(pin^F)^{2-}$ ligated to a metal center. We thus decided to optimize the geometries also in the presence of a point charge that mimicked a metal center with charges of +0.5, +1.0, +1.5, and +2.0. Indeed, these optimizations resulted in decreasing C_1-C_2 bond lengths of 1.711, 1.675, 1.656, and 1.642 Å respectively, as shown in Scheme 5. The corresponding O_1-C_1-C_2-O_2 torsion angles were observed to be -32.9°, -31.5°, -29.8°, and -27.4°. These features are much more consistent with experimentally observed structures.

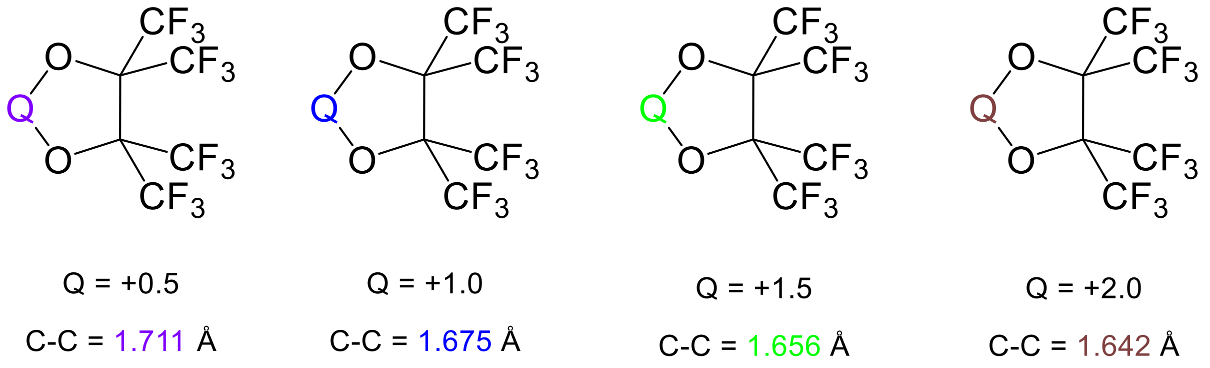

Scheme 5. Decrease in central C-C bond length in $\{Q(pin^F)\}$ with increase in formal charge on point charge Q.

Table 1. Summary of electronic structure features for **1** complexed to a series of five increasing point charges from 0 to + 2.0. Wiberg bond orders (WBO) and natural charges (NC) were calculated using unrelaxed MP2 densities, whereas NRT weights and delocalization energies were based on PBE0//MP2 results. The NRT % refers to the weight of all resonance structures in which the central C_1-C_2 bond has been broken.

Q	C_1-C_2 (Å)	C_1-C_2 WBO	C_1 NC	C_2 NC	NRT %	$\lvert n_O \rightarrow \sigma^* \rvert$ (kcal/mol)
0.0	1.761	0.72	0.14	0.14	30.6	39.3
+0.5	1.711	0.77	0.11	0.11	26.3	26.1
+1.0	1.675	0.81	0.05	0.12	20.0	18.7
+1.5	1.656	0.83	0.04	0.12	14.6	13.8
+2.0	1.642	0.85	0.04	0.09	13.0	10.0

The potential energy surface (PES) of the O_1-C_1-C_2-O_2 dihedral angle was also modeled while varying the point charge. The results are shown in Figure 4. We see here that for the uncomplexed dianion with Q = 0 (red in Figure 4), the conformation that we have been studying throughout this work is not the global minimum (Figure S1). We chose to use this conformation, however, due to its similarity with the experimental geometry. As point charges of increasing magnitude are included in the system, it can clearly be seen that the experimentally observed conformer

becomes more and more stable, and once the magnitude of the point charges reaches 2.0, there is only one unique minimum.

The most important electronic structure features of **1** complexed to point charges Q of various magnitudes are summarized in Table 1. It can be seen that all of these parameters follow the expected trend to approach crystallographically observed results as Q approaches +2.0. As the magnitude of the point charge increases, the natural charges of the $C_{1,2}$ atoms get more positive because in the presence of the additional positive charge the oxygen atoms are donating less charge to the C atoms alone. This effect is also clearly shown in the second-order perturbative estimates of the delocalization energy in the rightmost column resulting from interaction between the oxygen lone pairs and the C_1-C_2 σ* bond. This interaction has the added effect of reducing the weight of the resonance forms that break the central C_1-C_2 bond, thus increasing the C_1-C_2 bond order and shortening the bond length.

Summary

Over one hundred crystallographically-characterized transition metal, rare-earth, and *p*-block metal complexes of the perfluoropinacolate (pin^F) ligand have an exceptionally long central C-C bonds, averaging 1.63(3) Å. A computational study on a series of pinacolate ligands with varying degrees of fluorination (from four to zero CF_3 groups) has been carried out to understand the exceptionally long central C-C bonds in crystal structures with the perfluoropinacolate ligand, {A(pin^F)}. Two main influences are responsible: (i) negative hyperconjugation exists between the alkoxide O atom lone pairs and the central C-C σ* bond which also have resonance forms that "break" the central C-C bond and (ii) the lack of hydrogen bonding between any C-H bonds and the ligand O atoms. Steric influences do not play a significant role, but a central atom A with

a point charge of at least plus two bound to pin^F is required to reproduce the crystallographically determined C-C distances.

Acknowledgements

We thank all our colleagues in structural studies who provided the background data for this work, particularly Prof. Arnold Rheingold. PAH thanks the Boston University UROP program for support. The computational work reported in this paper was performed on the Shared Computing Cluster which is administered by Boston University's Research Computing Services. We are also grateful to Prof. John K. Snyder for thoughtful discussions and NSF CHE-2102532 for financial support.

References

1. Kotyk, C. M.; Weber, J. E.; Hyre, A. S.; McNeely, J.; Monteiro, J. H. S. K.; Domin, M.; Balaich, G. J.; Rheingold, A. L.; de Bettencourt-Dias, A.; Doerrer, L. H., Luminescence of Lanthanide Complexes with Perfluorinated Alkoxide Ligands. *Inorg. Chem.* **2020,** *59* (14), 9807-9823.
2. Elinburg, J. K.; Hyre, A. S.; McNeely, J.; Alam, T. M.; Klenner, S.; Pottgen, R.; Rheingold, A. L.; Doerrer, L. H., Formation of monomeric Sn(II) and Sn(IV) perfluoropinacolate complexes and their characterization by 119Sn Mossbauer and 119Sn NMR spectroscopies. *Dalton Trans.* **2020,** *49* (39), 13773-13785.
3. Elinburg, J. K.; Doerrer, L. H., Synthesis, structure, and electronic properties of late first-row transition metal complexes of fluorinated alkoxides and aryloxides. *Polyhedron* **2020,** *190*, 114765.
4. Elinburg, J. K.; Carter, S. L.; Nelson, J. J. M.; Fraser, D. G.; Crockett, M. P.; Beeler, A. B.; Nordlander, E.; Rheingold, A. L.; Doerrer, L. H., Reversible PCET and Ambient Catalytic Oxidative Alcohol Dehydrogenation by {V=O} Perfluoropinacolate Complexes. *Inorg. Chem.* **2020,** *59* (22), 16500-16513.
5. Brazeau, S. E. N.; Doerrer, L. H., Cu(I)-O2 oxidation reactions in a fluorinated all-O-donor ligand environment. *Dalton Trans.* **2019,** *48* (15), 4759-4768.
6. Steele, J. L.; Tahsini, L.; Sun, C.; Elinburg, J. K.; Kotyk, C. M.; McNeely, J.; Stoian, S. A.; Dragulescu-Andrasi, A.; Ozarowski, A.; Ozerov, M.; Krzystek, J.; Telser, J.; Bacon, J. W.; Golen, J. A.; Rheingold, A. L.; Doerrer, L. H., Square-planar Co(III) in {O4} coordination: large ZFS and reactivity with ROS. *Chem. Commun. (Cambridge, U. K.)* **2018,** *54* (85), 12045-12048.
7. Hannigan, S. F.; Arnoff, A. I.; Neville, S. E.; Lum, J. S.; Golen, J. A.; Rheingold, A. L.; Orth, N.; Ivanovic-Burmazovic, I.; Liebhaeuser, P.; Roesener, T.; Stanek, J.; Hoffmann, A.; Herres-Pawlis, S.; Doerrer, L. H., On the Way to a Trisanionic {Cu3O2} Core for Oxidase Catalysis: Evidence of an Asymmetric Trinuclear Precursor Stabilized by Perfluoropinacolate Ligands. *Chem. - Eur. J.* **2017,** *23* (34), 8320.
8. Tahsini, L.; Specht, S. E.; Lum, J. S.; Nelson, J. J. M.; Long, A. F.; Golen, J. A.; Rheingold, A. L.; Doerrer, L. H., Structural and Electronic Properties of Old and New A2[M(pinF)2] Complexes. *Inorg. Chem.* **2013,** *52* (24), 14050-14063.
9. Cantalupo, S. A.; Fiedler, S. R.; Shores, M. P.; Rheingold, A. L.; Doerrer, L. H., High-Spin Square-Planar CoII and FeII Complexes and Reasons for Their Electronic Structure. *Angew. Chem., Int. Ed.* **2012,** *51* (4), 1000.
10. Willis, C. J., Fluorinated Alcohols and Their Metal Complexes. *Coord. Chem. Rev.* **1988,** *88*, 133-202.
11. Popp, J.; Riggenmann, T.; Schroeder, D.; Ampssler, T.; Salvador, P.; Kluefers, P., Bent and Linear {CoNO}8 Entities: Structure and Bonding in a Prototypic Class of Nitrosyls. *Inorg. Chem.* **2021,** *60* (21), 15980-15996.
12. Heinemann, J.; Kluefers, P., [Ti(fpin)3]2-: a structurally characterized transition metal tris(perfluoropinacolato) complex. *Z. Anorg. Allg. Chem.* **2021,** *647* (18), 1815-1818.
13. Ampssler, T.; Monsch, G.; Popp, J.; Riggenmann, T.; Salvador, P.; Schroeder, D.; Kluefers, P., Not Guilty on Every Count: The "Non-Innocent" Nitrosyl Ligand in the Framework of IUPAC's Oxidation-State Formalism. *Angew. Chem., Int. Ed.* **2020,** *59* (30), 12381-12386.
14. Monsch, G.; Kluefers, P., [Fe(H2O)5(NO)]2+, the "Brown-Ring" Chromophore. *Angew. Chem., Int. Ed.* **2019,** *58* (25), 8566-8571.
15. Wurzenberger, X.; Neumann, C.; Kluefers, P., Enticing Cobalt into Planarity: Can a Pair of Diolato Ligands Make It Happen? *Angew. Chem., Int. Ed.* **2013,** *52* (19), 5159-5161.
16. Betz, R.; Kluefers, P., From simple diols to carbohydrate derivatives of phenylarsonic acid. *Inorg. Chem.* **2009,** *48* (3), 925-935.

17. Groom, C. R.; Bruno, I. J.; Lightfoot, M. P.; Ward, S. C., The Cambridge Structural Database. *Acta Crystallographica Section B* **2016,** *72* (2), 171-179.
18. Neese, F., The ORCA program system. *Wiley Interdisciplinary Reviews: Computational Molecular Science* **2012,** *2* (1), 73-78.
19. Neese, F., Software update: the ORCA program system, version 4.0. *Wiley Interdisciplinary Reviews: Computational Molecular Science* **2018,** *8* (1), e1327.
20. Neese, F., *ORCA – An Ab Initio, DFT and Semiempirical SCF-MO Package, Ver. 4.0*. Max Planck Institute for Chemical Energy Conversion: Mülheim a. d. Rurh, Germany, 2017.
21. Neese, F.; Wennmohs, F.; Becker, U.; Riplinger, C., The ORCA quantum chemistry program package. *The Journal of Chemical Physics* **2020,** *152* (22), 224108.
22. Grimme, S., Improved second-order Møller–Plesset perturbation theory by separate scaling of parallel- and antiparallel-spin pair correlation energies. *The Journal of Chemical Physics* **2003,** *118* (20), 9095-9102.
23. Gerenkamp, M.; Grimme, S., Spin-component scaled second-order Møller–Plesset perturbation theory for the calculation of molecular geometries and harmonic vibrational frequencies. *Chem. Phys. Lett.* **2004,** *392* (1), 229-235.
24. Grimme, S., Improved third-order Møller–Plesset perturbation theory. *J. Comput. Chem.* **2003,** *24* (13), 1529-1537.
25. Zheng, J.; Xu, X.; Truhlar, D. G., Minimally augmented Karlsruhe basis sets. *Theor. Chem. Acc.* **2011,** *128* (3), 295-305.
26. Weigend, F.; Ahlrichs, R., Balanced basis sets of split valence, triple zeta valence and quadruple zeta valence quality for H to Rn: Design and assessment of accuracy. *Physical Chemistry Chemical Physics* **2005,** *7* (18), 3297-3305.
27. Stoychev, G. L.; Auer, A. A.; Neese, F., Automatic Generation of Auxiliary Basis Sets. *Journal of Chemical Theory and Computation* **2017,** *13* (2), 554-562.
28. Glendening, E. D.; Badenhoop, J. K.; Reed, A. E.; Carpenter, J. E.; Bohmann, J. A.; Morales, C. M.; Karafiloglou, P.; Landis, C. R.; Weinhold, F. *NBO 7.0*, Theoretical Chemistry Institute, University of Wisconsin: Madison, WI, 2018.
29. Lu, T.; Chen, F., Multiwfn: A multifunctional wavefunction analyzer. *J. Comput. Chem.* **2012,** *33* (5), 580-592.
30. Nikolaienko, T. Y.; Bulavin, L. A.; Hovorun, D. M., JANPA: An open source cross-platform implementation of the Natural Population Analysis on the Java platform. *Computational and Theoretical Chemistry* **2014,** *1050*, 15-22.
31. Nikolaienko, T. Y.; Bulavin, L. A., Localized orbitals for optimal decomposition of molecular properties. *Int. J. Quantum Chem* **2019,** *119* (3), e25798.
32. Angeli, C.; Cimiraglia, R.; Evangelisti, S.; Leininger, T.; Malrieu, J. P., Introduction of n-electron valence states for multireference perturbation theory. *The Journal of Chemical Physics* **2001,** *114* (23), 10252-10264.
33. Brazeau, S. E. N.; Pope, F.; Huang, V. L.; Anklin, C.; Rheingold, A. L.; Doerrer, L. H., Phosphine ligands as protecting groups for 3d complexes in oxidation by O2. *Polyhedron* **2020,** *186*, 114609.
34. Raabe, G.; Gais, H.-J.; Fleischhauer, J., Ab Initio Study of the Effect of Fluorination upon the Structure and Configurational Stability of α-Sulfonyl Carbanions: The Role of Negative Hyperconjugation. *Journal of the American Chemical Society* **1996,** *118* (19), 4622-4630.
35. Exner, O.; Böhm, S., Negative hyperconjugation of some fluorine containing groups. *New Journal of Chemistry* **2008,** *32* (8), 1449-1453.
36. Oomens, J.; Berden, G.; Morton, T. H., Negative Hyperconjugation versus Electronegativity: Vibrational Spectra of Free Fluorinated Alkoxide Ions in the Gas Phase. *ChemPhysChem* **2015,** *16* (9), 1992-1995.